A NUMERICAL INVESTIGATION OF THE INFLUENCE OF ACTIVE CONTROL MOVEMENTS ON VIBRATION AND BVI-NOISE

S. Schlechtriem, D. Nellessen, J. Ballmann
Lehr- und Forschungsgebiet für Mechanik, RWTH Aachen, Germany

1. Abstract

The interactions of the rotor-blade with the tip vortices of the preceding blades can cause a significant increase in noise and vibration. Especially during descent flight conditions at advance ratios of 0.1 - 0.2, BVI is the major source of noise and has an effect on vibratory airloads also. Active control systems like HHPC and IBC have been developed during the last years. Their control movements influence the rotor-blade's motion in an appropriate way to minimize vibration and to reduce BVI-noise. Concerning the application of the active control devices the question arises : Which active control movement (amplitude and time history) introduced via the pitch horn is most efficient ?
The numerical investigation described in this article is intended to make a contribution to answer this question. All the computations have been carried out using the SOFIA (Solid-Fluid-Interaction) code which was developed to analyze aerodynamic and aero-elastic phenomena.

2. List of Symbols

FLOW PART:

c	chord length
C_L	lift coefficient
C_M	moment coefficient
e	total specific energy
M	Mach number
p	pressure
$\mathbf{v}$	flow velocity
λ	velocity of the grid (components $\dot{x}$, $\dot{y}$, $\dot{z}$)
ρ	density
Γ	circulation
ψ	rotor azimuthal angle
V	volume
$\mathbf{n}$	normal vector

Indices:

∞	infinity
w	vortex position
i, j, k	space directions
μ, γ	iteration indices

STRUCTURAL PART:

$\mathbf{a}$	acceleration
EA	tension stiffness
$\mathbf{EI}$	bending stiffness matrix
$\mathbf{GA}$	shear stiffness matrix
GI_T	torsional stiffness
$\mathbf{M}$	moment
N	normal force
$\mathbf{q}$	transverse load per unit length
$\mathbf{Q}$	shear force
$\mathbf{u}$	displacement
φ	rotation by deformation
γ	shear angle
ρI	rotatory inertia
ρA	mass per length
ω	angular velocity
Ω	tensor of angular velocities
m	torsional moment per unit length

Indices:

A	input kinematics (RA main rotor axis, cA cyclic pitch variation)
B	bending, bending centre
C	cross-sectional centre of gravity
D	shear centre
CD,CB	distances between centres
T	torsion

3. Introduction

The major task concerning the investigation of BVI is the prediction of the unsteady flow phenomena on the advancing side of the rotor. Here the blade-vortex interactions are most intense at azimuthal angles between 20 and 70 degrees. In the past experiments and numerical investigations have been carried out by Meier et al /1/,/2/, Caradonna et al /3/, /5/,/13/, Galbraith et al /4/, McCroskey et al /6/, Ballmann et al /7/, /8/, /9/ to study the BVI mechanism. They show that the fundamental phenomena are understood and that even very detailed information about the whole pressure field is now available as will be shown later on.
With the development of active control systems like Higher Harmonic Pitch Control /10/ and Individual Blade Control /11/ it is possible to influence the rotor-blade's motion to minimize the BVI noise. The earlier mentioned question concerning the most efficient control movement at the pitch horn needs to be particularized. First of all one can ask: How should one cross-section close to the rotor-blade's tip move during a blade-vortex interaction? Concerning this first problem two-dimensional computations have been performed to get an idea of appropriate blade motions. The realization of those movements via additional pitch motions at the blade's root is even more complex. As the blade is flexible the desired change of the angle of attack close to the blade's tip lags behind the control movement at the blade's root. The calculation of this time lag which depends on the wave propagation speed of the torsional mode is the second problem. To investigate the whole aeroelastic problem a three-dimensional study is necessary which have been performed with the SOFIA code /9/.
SOFIA consists of a fluid solver (INFLEX) and a structural solver (ODISA). A brief description of the two modules - INFLEX for the flow analysis and ODISA (One-Dimensional Structural Analysis) for the structural analysis - that are required to accomplish BVI computations for rigid and especially elastic rotor-blades is provided. The basic algorithm of the INFLEX code was developed by Eberle and Brenneis /12/ .

3. Physical Model

Flowfield

Unsteady flow phenomena like strong acoustic waves and moving shock waves occur on the advancing side of the rotor where the intensive BVI takes place at azimuthal angles between 20 and 70 degrees. As the flow is attached in this regime, viscosity effects are neglected. For the computation of the unsteady, compressible flow about the elastic rotor-blade the Euler equations

$$\frac{d}{dt}\int_{V(t)} \rho dV + \int_{\partial V(t)} \rho (\mathbf{v} - \Lambda)\cdot \mathbf{n} dS = 0 \quad , \tag{1}$$

$$\frac{d}{dt}\int_{V(t)} \rho \mathbf{v} dV + \int_{\partial V(t)} \mathbf{v}\,[\rho(\mathbf{v} - \Lambda)\cdot \mathbf{n}]dS = -\int_{\partial V(t)} p\mathbf{n} dS \quad , \tag{2}$$

$$\frac{d}{dt}\int_{V(t)} e dV + \int_{\partial V(t)} e\,(\mathbf{v} - \Lambda)\cdot \mathbf{n} dS = -\int_{\partial V(t)} p\,(\mathbf{v}\cdot \mathbf{n})\,dS \tag{3}$$

are solved with respect to an inertial reference system for time dependent non material balance volumes. In the above equations the velocity of the surface of the balance volume is denoted λ. This velocity takes the rotation of the rotor-blade, the cyclic pitch variation as well as the blade's deformation into account.

Deformation of the Rotor-Blade

As the aspect ratio of a rotorblade is high a beam theory is used for the description of the unsteady blade deformation. In order to estimate the dynamical behaviour of the blade correctly, a wave mechanical model is introduced. Timoshenko's theory of beams is applied. A material cross- section of the beam has three translational and three rotational (one torsional and two bending) degrees of freedom. In general the lines which connect the centers of mass, bending and twist do not coincide. The calculation of the structural deformation is performed in the rotating frame. Assuming the deformations in the rotating frame to be small, the governing equations can be linearized. Due to the 6 DOF (rotation, translation) of a beam's cross section, the governing equations are the equation of momentum

$$\rho A a'_C = \frac{\partial}{\partial \xi_1} (N + Q) + q \quad , \tag{4}$$

where a'_C is the acceleration of the centre of gravity of a material cross-sectio

$$a'_C \doteq a'_O + a_C + \xi_{C\alpha} \dot{\omega} \wedge e_\alpha + \xi_1 \omega_A \wedge (\omega_A \wedge e_1) \quad , \qquad \alpha = 2, 3$$

with

$$\omega = \dot{\varphi} + \omega_A \quad , \qquad \omega_A = \omega_{RA} + \omega_{cA} \quad .$$

and the equation of moment of momentum for $\dot{\omega}_{RA} = 0$

$$\begin{aligned} \rho I_C (\dot{\varphi}' + \dot{\omega}_{cA}) \doteq & \frac{\partial}{\partial \xi_1} (M_T + M_B) + m - \omega_A \wedge [\rho I_C (\omega_A + \dot{\varphi})] \\ & + \frac{\partial}{\partial \xi_1} (\xi_{CD\alpha} e_{s\alpha} \wedge Q + \xi_{CB\alpha} e_{s\alpha} \wedge N) \\ & + \left[e_1 + \frac{\partial}{\partial \xi_1} (\xi_{CB\alpha} e_{s\alpha} + u) \right] \wedge (N + Q) \quad , \qquad \alpha = 2, 3 \quad . \end{aligned} \tag{5}$$

The kinematical approximation for the deformation part of the blade motion is given by

$$u_D = u + \varphi \wedge \xi_{D\alpha} e_\alpha \quad ; \qquad \alpha = 2, 3$$

$$\gamma_2 = u_{2,\xi_1} - (\varphi_T \xi_{D3})_{,\xi_1} - \varphi_{B3} \; ; \quad \gamma_3 = u_{3,\xi_1} - (\varphi_T \xi_{D2})_{,\xi_1} - \varphi_{B2} \; . \tag{6}$$

Constitutive equations within the scope of Timoshenko's approximation are

$$N = EA u_{1,\xi_1} e_1, \; Q = GA\mathcal{K}\gamma \; , \; M_T = GI_T \varphi_{T,\xi_1} e_1 \; , \; M_B = EI \varphi_{B\alpha,\xi_1} e_1 \; , \quad \alpha = 2, 3 \; . \tag{7}$$

Coupling of the Equations

The equations describing the flowfield and the structural deformation are coupled. The deformation depends on the aerodynamic load which is taken into account on the right hand side of the structural equations. On the other hand the flowfield depends on the actual deformation because the flow velocity perpendicular to the rotor-blade's surface has to be zero consistently .

Due to the actual deformation of the rotor-blade the inner boundary of the flowfield which represents the surface of the rotor-blade is moved. For the numerical solution of the Euler equations the flowfield is devided up into finite volumes. While the surfaces of the volumes at the outer boundary are moved due to the rotation only, the surfaces of the volumes at the inner boundary experience the additional elastic movement of the rotor-blade's surface. All the volumes within the flowfield are rearranged in such a way that the structure of the numerical grid remains unchanged. Therefore, the velocity λ of the surface of the balance volumes consists of two parts

$$\lambda = \lambda^{el}(C_L, C_D, C_M) + \lambda^{rot}(t) \quad .$$

The rotational velocity λrot is a known time dependent function. The velocity λel occurs because of the elastic deformation at the inner boundary and is a result of the calculation of the structural deformation. At the outer boundary this velocity is zero and throughout the flowfield it varies due to the rearrangement of the numerical grid.

Vortex

A Lamb-Oseen vortex is introduced into the undisturbed flowfield some chord lengths in front of the rotor-blade. The vortex rotates clockwise and passes the rotor-blade at the lower side.

4. Solution Strategy

The equations describing the flowfield and the structural deformation are integrated with respect to time simultaneously . The flow-chart in Figure 1 illustrates the solution strategy:

The main time loop consists of three fundamental parts. ODISA calculates the deformation of the rotor-blade, which depends on the current airload.

The points at the inner boundary of the numerical grid of the flowsolver representing the surface of the rotorblade are moved due to the calculated deformation of the rotor-blade. This is done by GRIDGEN (GRID GENerator). All grid points are rotated about the helicopter's main rotor axis. Finally, the grid points within the flowfield are rearranged by GRIDGEN.

In the third part of SOFIA the flowfield is calculated.
In Figure 1 the rotating frame is denoted by 1',2' and 3' and the cross-section fixed frame is denoted 1,2 and 3. The rotor-blade is shown in a non deformated reference configuration at time level zero and for the actual configuration at time level n and (n+1). The actual configuration is determined by the vector of displacement of each cross- section and by the rotating of the cross-section. These vectors are calculated by ODISA as a function of the spanwise direction. After moving all the grid points in the prescribed way, the flowfield is calculated for the new configuration and the airloads can be determined.

Numerical Method: Calculation of the Structural Deformation

The equations of momentum, of moment of momentum and the constitutive equations can be transformed into a system of 12 linear, first order, partiell differential equations (PDEs) which is of hyperbolic type. This system of PDEs is transformed into its canonical form. Riemann invariants are used. The compatibility relations are integrated by Heun's method. Each Riemann invariant is treated in its own numerical grid. The CFL- number in each grid is per construction one. For a detailed description of the numerical method see references /9/.
As an alternative to the method of characteristics a finite element method has been developed for the Timoshenko beam: A system of ordinary differential equations (ODEs) which is second order in time to determine the generalized deflections is derived by applying Hamilton's principle and the method of Ritz/Kantorowitsch. Linear damping is included. Discretization is done by isoparametric, two noded elements. The set of ODEs is integrated by Newmark's method, where the resulting linear system of equations is solved directly with a LU- decomposition. The external forces are assumed to vary linearly in one time-step. Alternatively, the system of ODEs is diagonalized by solving the generalized eigenvalue problem (EVP) and the time integration is done by the evaluation of Duhamel's integral (Rayleigh- damping). The increment of Duhamel's integral for the current time-step is calculated analytically.

Numerical Method: Calculation of the Flowfield

For the numerical integration of the strong conservation form of the Euler equations an implicit relaxation scheme is used. The unfactored Euler equations are solved by applying a Newton method. Relaxation is performed with a point Gauss-Seidel algorithm. The combination of a Newton method with a point Gauss- Seidel algorithm leads to a robust numerical scheme. Concerning the resolution of pressure and shock waves a characteristic variable splitting technique is employed.

Numerical Method: Grid-Generation

An elliptic grid generator is employed to calculate the grid at each time step. A system of 3 elliptic differential equations (DEs) of 2nd order (Poisson- and Laplace- equation) is solved. The DEs are approximated by central difference schemes. The resulting linear equation system is solved iteratively by applying a Gauss- Seidel- algorithm. As each grid deviates only slightly from the grid at the preceding time step, only few iterations are necessary.

5. Results

As mentioned above the parallel blade-vortex-interaction has been investigated by many researchers and a lot of computational and experimental results are available to compare with. Recently an experimental study of rotor-blade-vortex interaction (BVI) aerodynamics and acoustics was carried out by F.X. Caradonna /13/ in NASA Ames 80 by 120 Foot Wind Tunnel. The vortex was generated externally and interacts with the two-bladed rotor at zero thrust. During the BVI several propagative and convective events occur and the ability to predict these events is a good accuracy test for a CFD method. The computation is initialized by computing a steady state solution and introducing the vortex 4 chord lenghts in front of the airfoil's leading edge. A Lamb type model is used to describe the initial structure of the vortex. Figure 2 shows the experimental blade pressure variations induced by BVI and the comparison with our computations. The results are very promising and all the important flow features especially the propagative events /9/ are captured.

Based on these preliminary computations, the influence of the rotorblade's elasticity on the BVI has been studied. Figures 3 to 8 show some typical results. The whole unsteady data have been analyzed and put on video. The acoustic wave propagation phenomena are enlightend and the effect of the elastic deformation on the transient pressure field can be seen. Within a two-dimensional analysis two parameters concerning the material properties are of importance: the reduced frequency k and a second similarity parameter namely the ratio of the mean density of one cross-section and the density of the surrounding fluid, which will be called inertia parameter further on. The Figures 3 and 4 show results for a clockwise rotating vortex which passes the elastically suspended airfoil at the lower side and induces a downwind. In Figures 3 two pressure distributions for a plunging airfoil are given. Due to the induced downwind the airfoil moves downwards. When the vortex passes the airfoil an upwind is induced and with a certain time lag -depending on the inertia number- the sign of the blade's vertical velocity changes. Concerning the wave phenomena two effects predominate: 1. The distance between the airfoil and the vortex core is reduced (this amplifies the interaction) and 2. The vertical velocity of the airfoil is negative and induces an angle of attack which compensates partly the angle of attack induced by the vortex (this reduces the strength of the interaction). But the angle of attack induced by the blade's vertical velocity depends on time only, while the one induced by the vortex is a function of space also. In Figures 4 results concerning computations for the case of a pitching airfoil are shown, where the axis of rotation is chosen to be either at the leading or at the trailing edge. If the rotational axis is at $x/c = 0$, the downwind induces a positive moment and the compressibility as well as the transonic wave can be reduced.

The computations show that a reduction of BVI-noise is possible only for extrem values of the inertia parameter /9/. As the values for the density of conventional rotor-blades are an order of magnitude higher than the minimum values which are

required to show any noise reduction, any efforts concerning the modification of material properties are expected to have a minor effect on noise reduction. But nevertheless the pressure distributions shown in Figures 3 and 4 confirm that the wave phenomena of a BVI can be influenced by a blade motion and that the study of the blade's elastic motion can give valuable ideas how to apply active control movements, even if the material properties of the blade are not realistic.
An analysis of a complete three-dimensional interaction of a vortex with an elastic rotor-blade (Figure 7) was performed. The three-dimensional results confirm the two-dimensional compuations and the typical lift distribution due to BVI can be observed (Figure 6). Furthermore the three-dimensional results demonstrate the impact of BVI on vibration. The influence of the torsional motion on the lift distribution is obvious. The weak damping of the torsional motion is remarkable.
Figure 10 shows the pressure field about a rotating blade for hover and forward flight conditions. Similar to the computations of /15/, /16/ a fully converged periodic solution has been calculated.
Based on this investigation further three-dimensional computations will be carried out to determine control movements via the pitch horn to reduce BVI-noise.

6. Summary

The SOFIA code has been applied to predict the influence of blade deformations and control movements on noise and vibration during BVI. A description of SOFIA's two modules - INFLEX for the flow analysis and ODISA for the structural analysis - that are required to accomplish BVI computations is provided. The detailed investigation of the wave propagation phenomena during BVI and the comparison with experimental data is very promising. Furthermore the computations give an answer to the question which active contol movements can indeed lead to a reduction of BVI-noise.

7. Acknowledgements

This work was partially supported by the Deutsche Forschungsgemeinschaft and the U.S. Government through its European Research Office. We would like to thank Dr. A. Brenneis and Dr. A. Eberle from the DASA for the provision of the computer code INFLEX. Computations were performed using the facilities of the Rechenzentrum der RWTH Aachen.

8. Literature

1. G.E.A. Meier and R. Timm, Unsteady Vortex Airfoil Interaction, AGARD CP-386, 1985, 16.1-16.10
2. K. Ehrenfried and G.E.A. Meier, Numerical Investigation of the Basic Mechanisms of BVI-Noise Generation, 19th European Rotorcraft Forum, Paper No. B9, 1993
3. F.X., Caradonna, R.C. Strawn and J.O. Bridgeman, An Experimental and Computational Study of Rotor-Vortex Interactions, 14th European Rotorcraft Forum, 1988
4. M.H. Horner, E. Saliveros and R.A. Mc. D. Galbraith, An Experimental Investigation of the Oblique Blade-Vortex Interaction, 17th European Rotorcraft and Lift Aircraft Forum, Berlin, Germany, Sept. 1991
5. H.E. Jones and F.X. Caradonna, Full-Potential Modelling of Blade-Vortex Interactions, 12th European Rotorcraft Forum, Paper No. 27, 1986
6. G.R. Srinivasan, W.J. McCroskey and J.D. Baeder, Aerodynamics of Two-Dimensional Blade-Vortex Interaction, AIAA-Journal, Vol. 24, No. 10, Oct. 1986
7. J. Ballmann and C. S. Kocaaydin, Some Aerodynamic Mechanisms of Impulsive Noise during Blade-Vortex-Interaction, 16th European Rotorcraft Forum,1990
8. S. Körber and J. Ballmann, Aerodynamik und Aeroakustik bei Wirbel-Profil-Wechselwirkungen, 8. DGLR Fachsymposium, Strömungen mit Ablösungen, 1992
9. S. Schlechtriem, D. Nellessen and J. Ballmann: Elastic Deformation of Rotor-Blades Due to BVI, 19th European Rotorcraft Forum, Paper No. B1, 1993
10. W.R. Splettstoesser, K.-J. Schultz, R. Kube, T.F. Brooks, E.R. Booth, G. Niesl and O. Streby, BVI Impulsive Noise Reduction By Higher Harmonic Pitch Control: Results Of A Scaled Model Rotor Experiment In The DNW, 17th European Rotorcraft Forum, 1991
11. P. Richter and H.D. Eisbrecher, Design and First Tests of Individual Blade Control Actuators , 16th European Rotorcraft Forum, 1990
12. A. Brenneis and A. Eberle, Application of an Implicit Relaxation Method Solving the Euler Equations for Time-Accurate Unsteady Problems, Journal of Fluids Engineering, Vol. 112, Dec 1990, pp 510-520
13. C. Kitaplioglu and F.X. Caradonna, Aerodynamics and Acoustics of Blade-Vortex Interaction Using an Independently Generated Vortex, paper presented at the American Helicopter Aeromechanics Specialists Conference, San Francisco, 1994
14. D. Nellessen, S. Schlechtriem and J. Ballmann, Numerical Simulation of Flutter Using the Euler Equations, Notes on Numerical Fluid Mechanics, 1992
15. K. Ramachandran, S. Schlechtriem, F.X. Caradonna, J. Steinhoff, The Application of Vorticity Embedding to the Computation of Advancing Rotor Flows, presented at the 49th AHS Annual Forum, St. Louis, MO, 1993
16. K. Ramachandran, S. Schlechtriem, F.X. Caradonna, J. Steinhoff: " Free-Wake Computation of Helicopter Rotor Flowfields in Forward Flight ", AIAA - 93 - 3079, 1993

Flow chart SOFIA

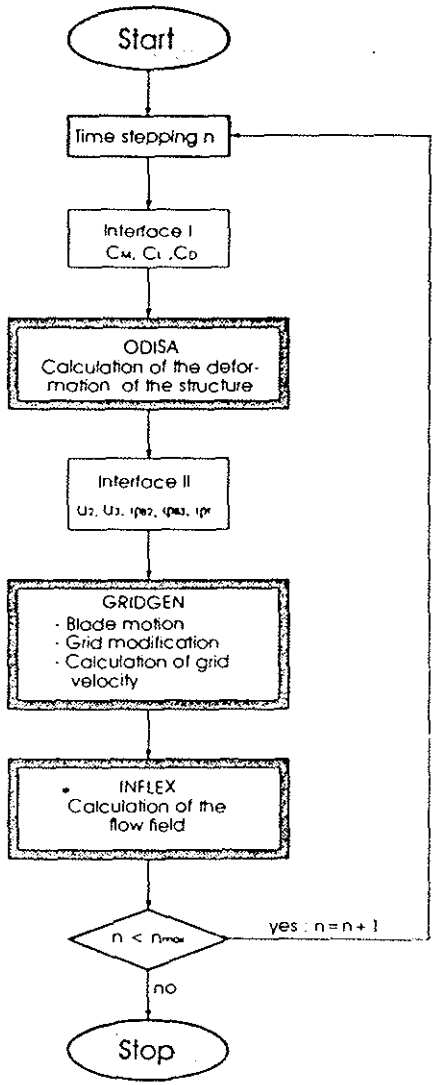

Figure 1: SOFIA Flow Chart

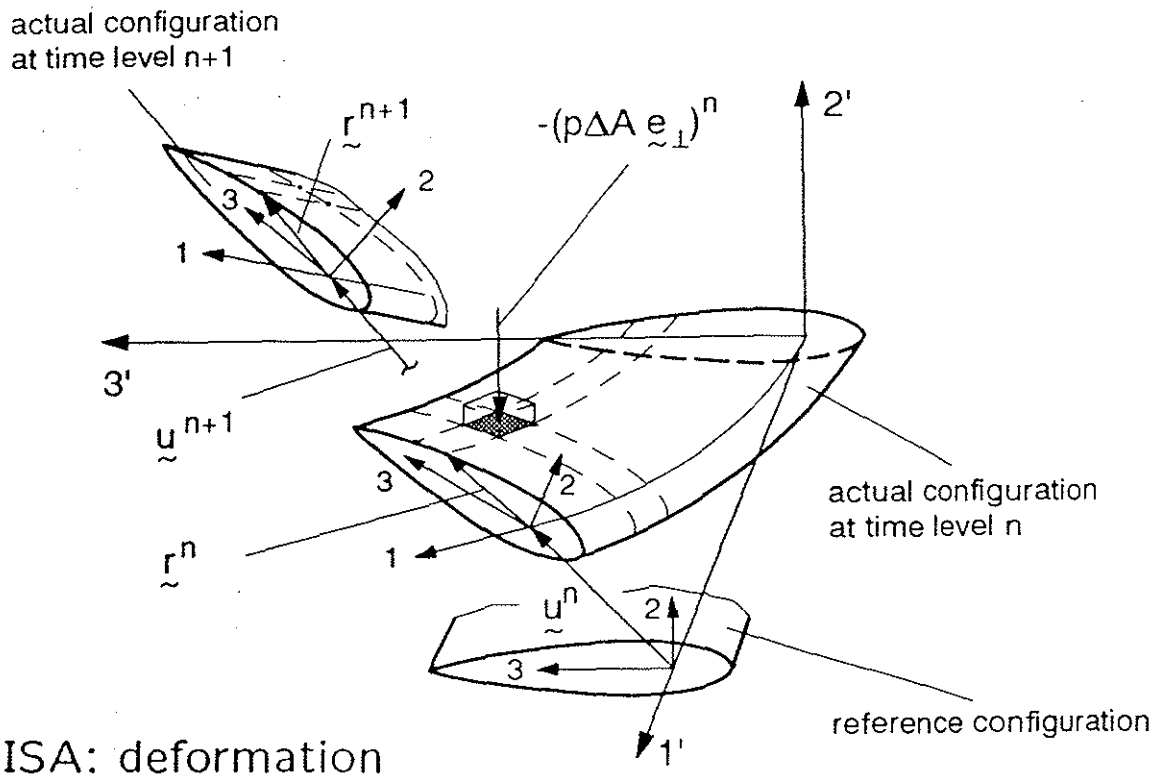

- ODISA: deformation

$$\Rightarrow \mathbf{u}^{n+1}, \mathbf{r}(\varphi^{n+1})$$

- GRIDGEN

- INFLEX: flowfield

$$\Rightarrow -(p\Delta A\mathbf{e}_\perp)^{n+1}$$

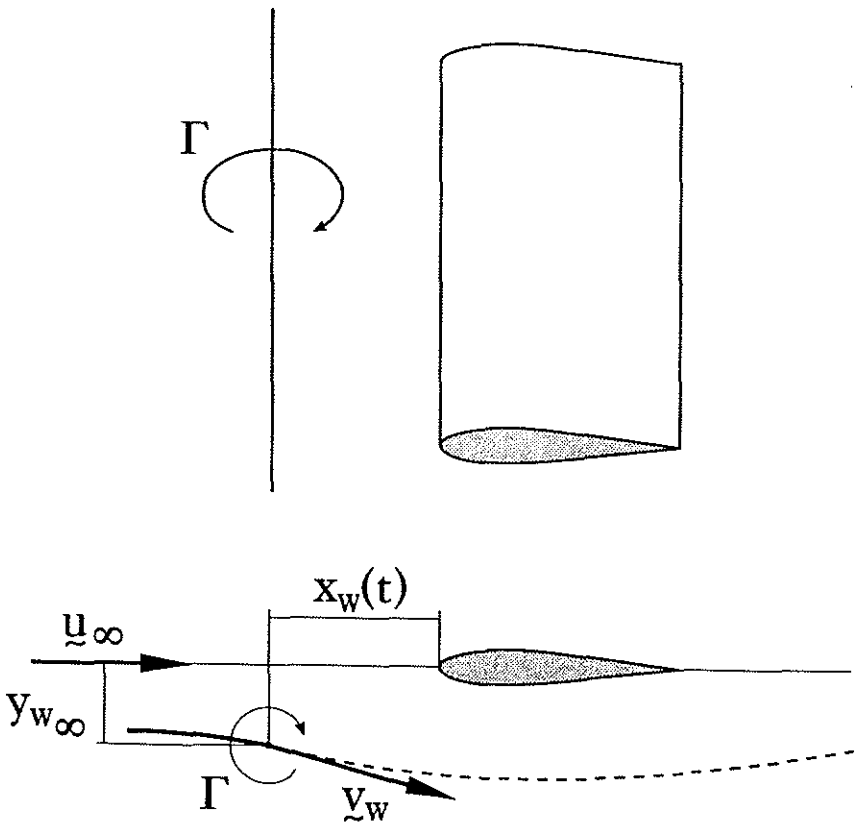

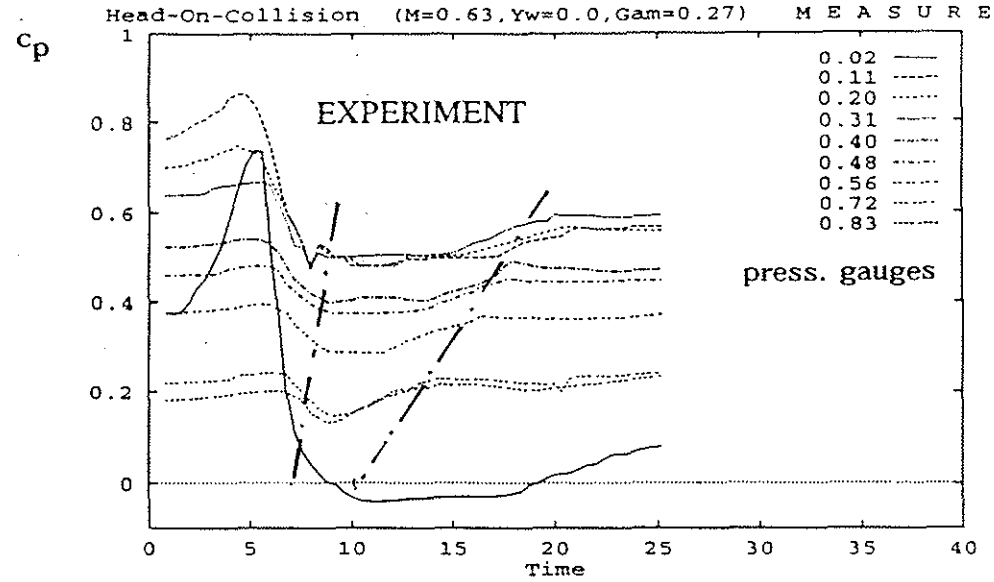

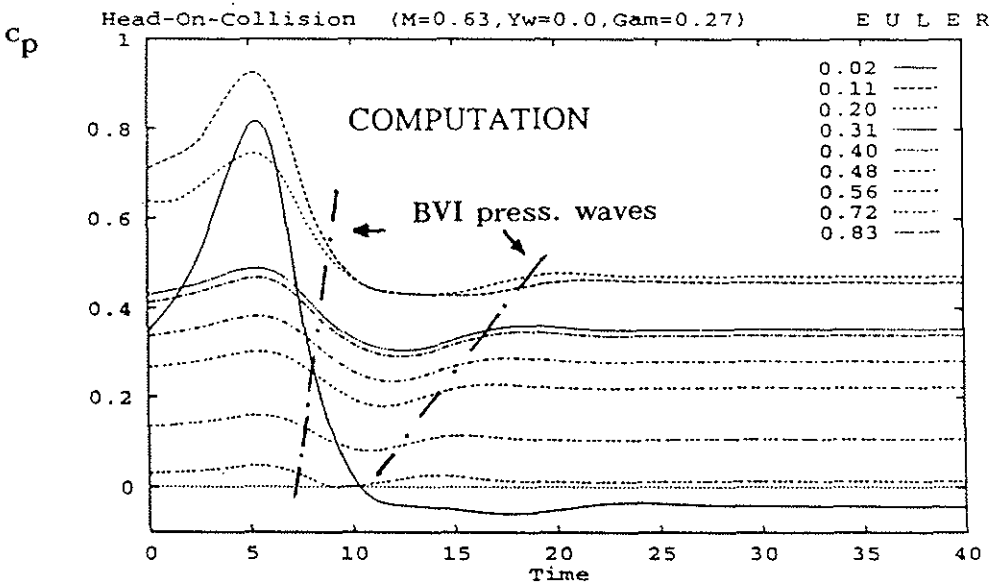

Figure 2: Comparison of experiments and numerical simulation for a parallel blade-vortex interaction on the rotor-blade's upper side (M=0.63, y_w = 0. , Γ = 0.27)

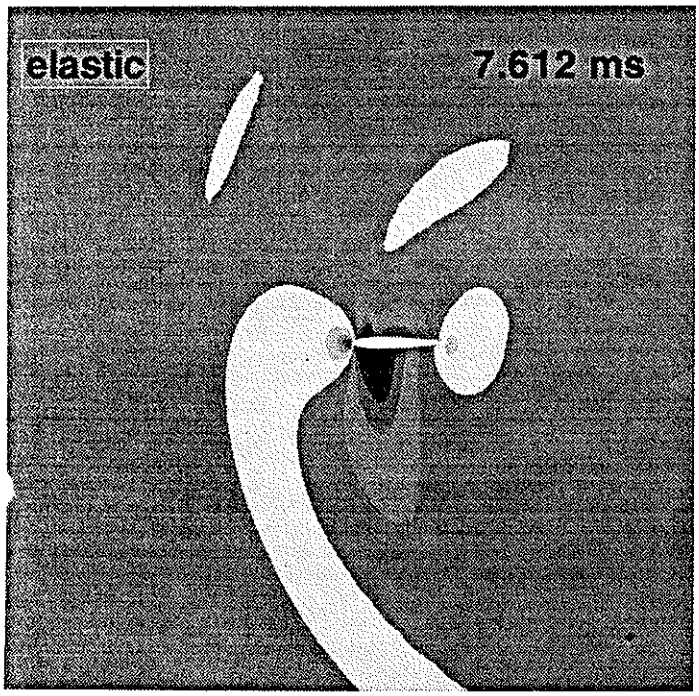

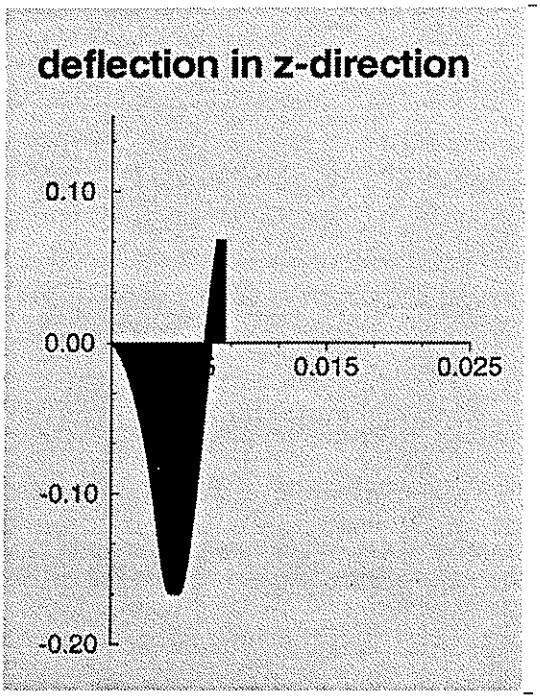

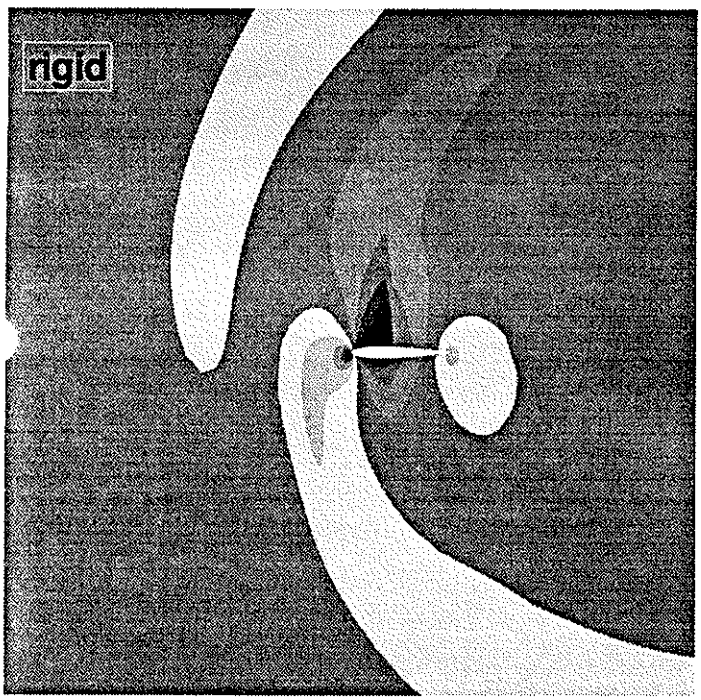

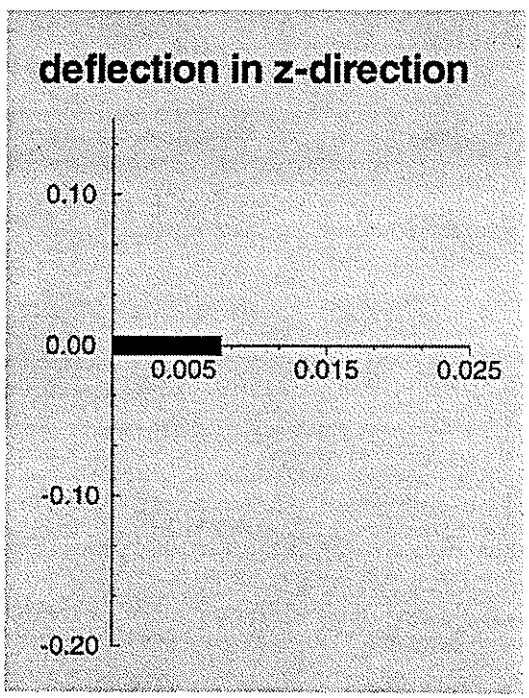

Figure 3a: Typical results of a BVI computation (rigid versus flexible blade, 1DOF: plunge); M=0.73, y_W=0.26, Γ=0.8, k=0.58

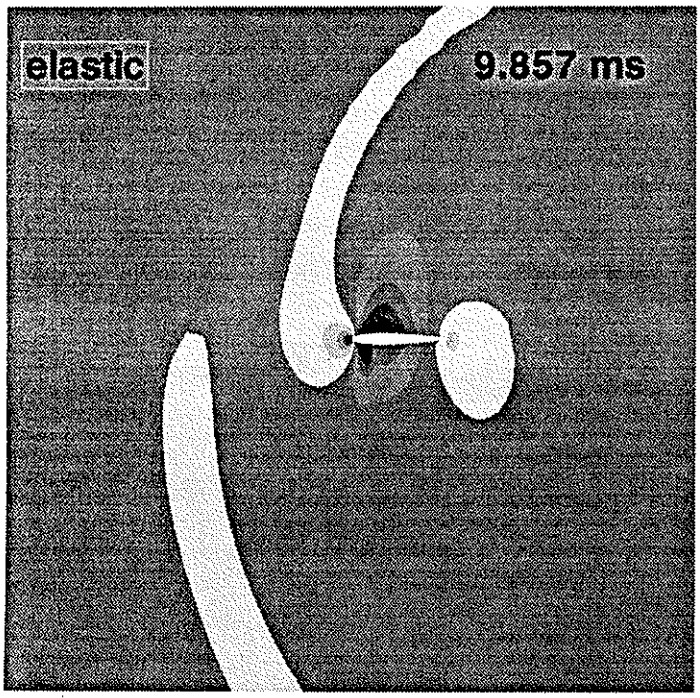

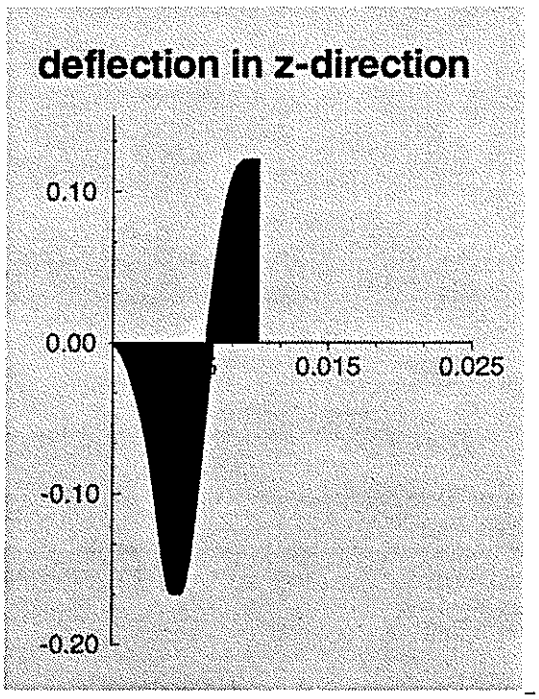

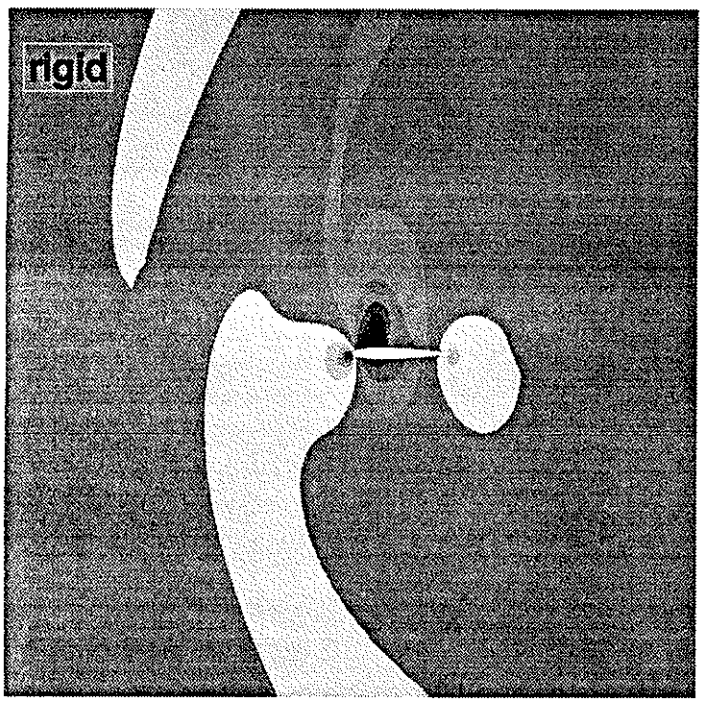

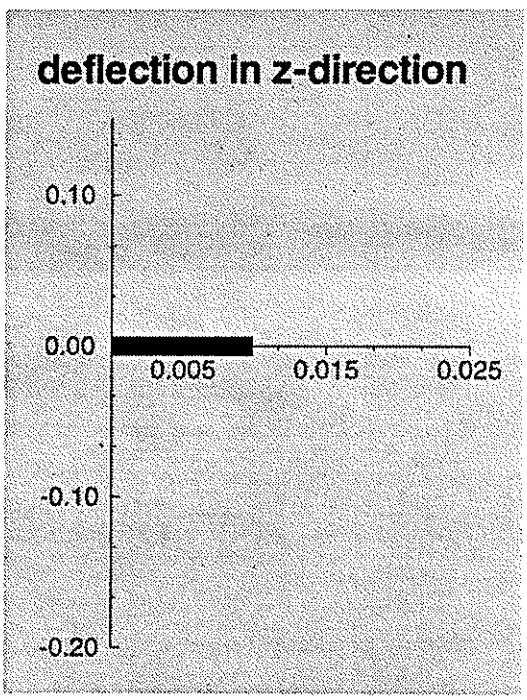

Figure 3b: Typical results of a BVI computation (rigid versus flexible blade, 1DOF: plunge); M=0.73, y_W=0.26, Γ=0.8, k=0.58

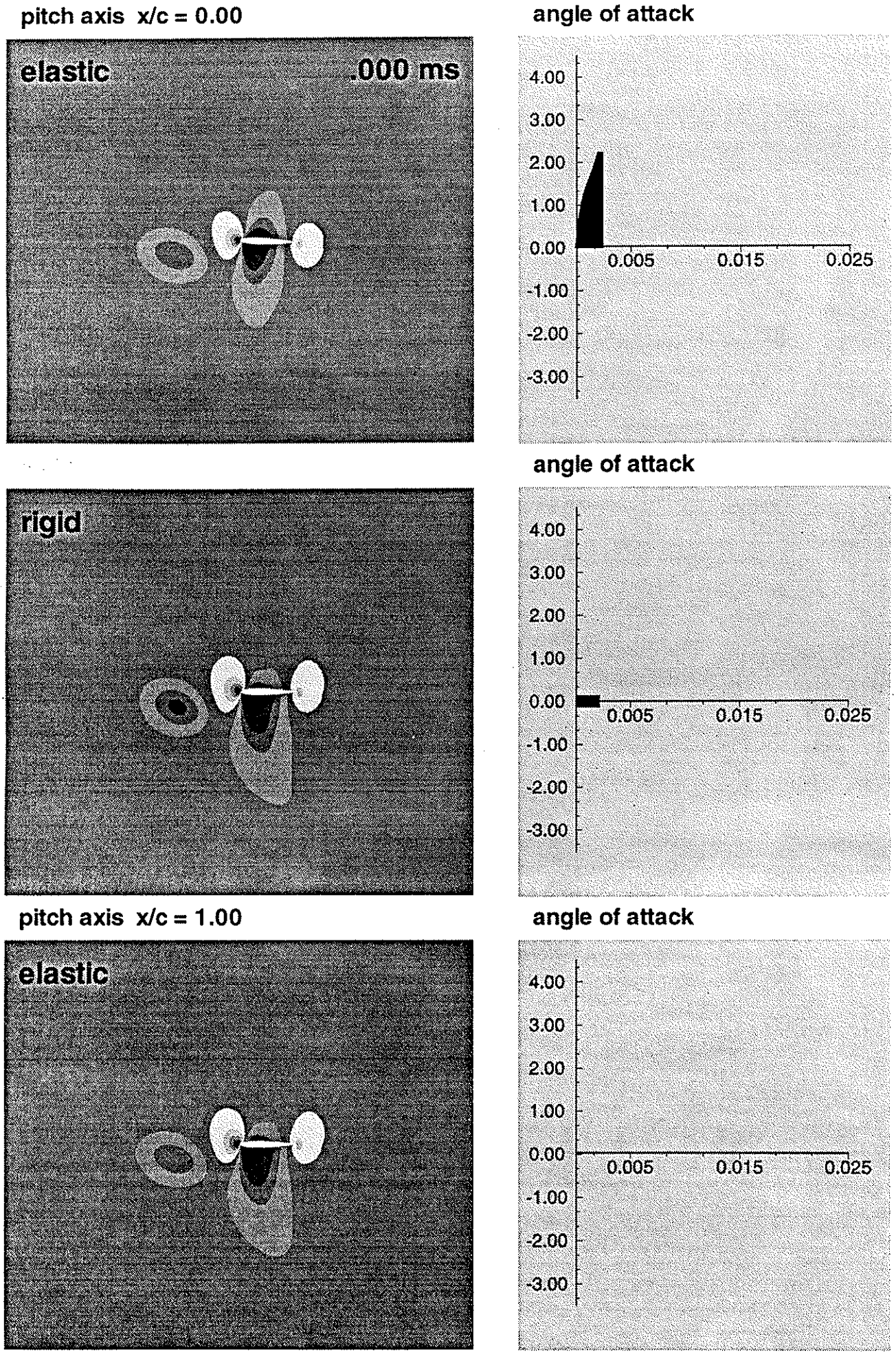

Figure 4a: Typical results of a BVI computation (rigid versus flexible blade, 1DOF: pitch); M=0.73, y_w=0.26, Γ=0.8, k=0.21

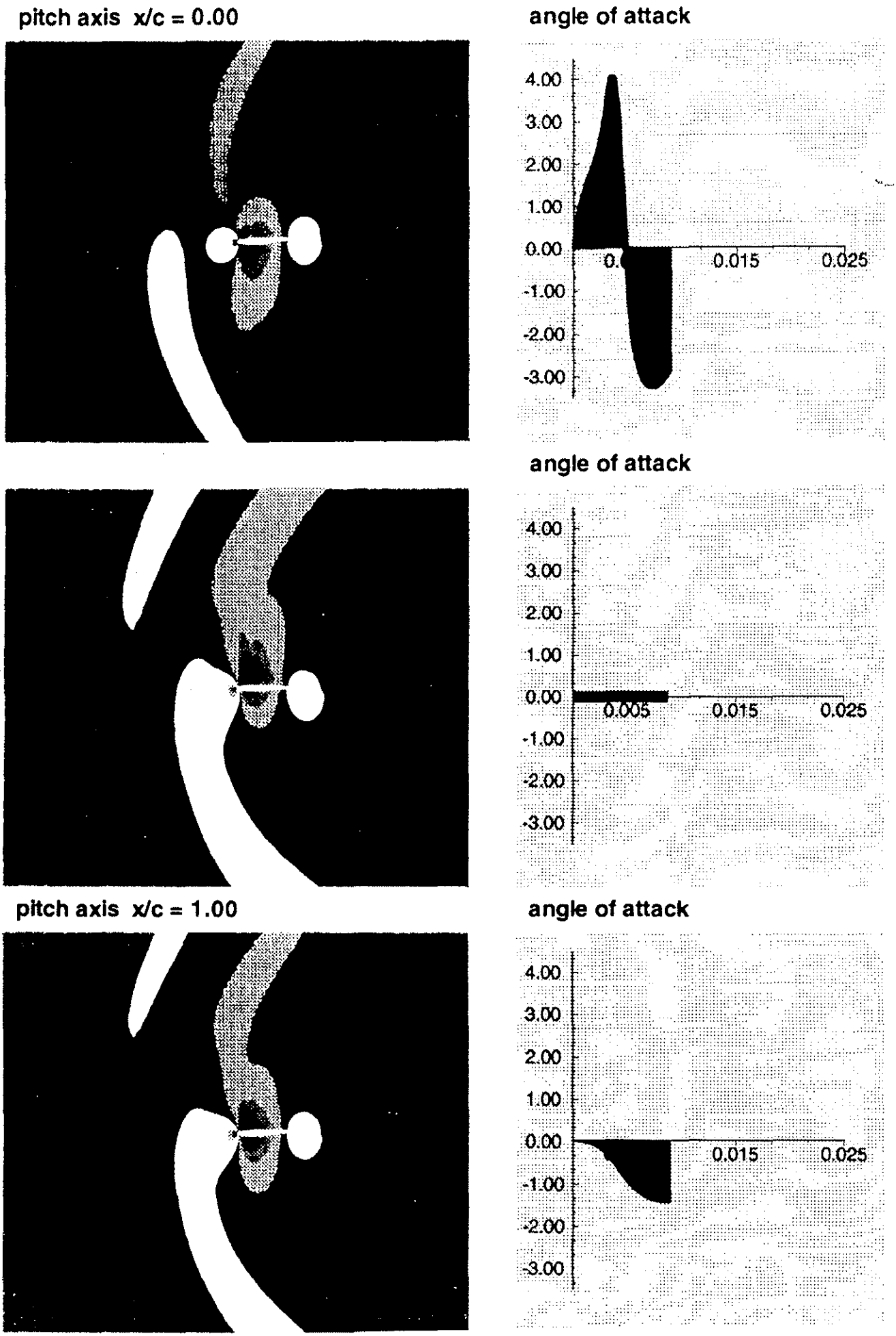

Figure 4b: Typical results of a BVI computation (rigid versus flexible blade, 1DOF: pitch); M=0.73, y_W=0.26, Γ=0.8, k=0.21

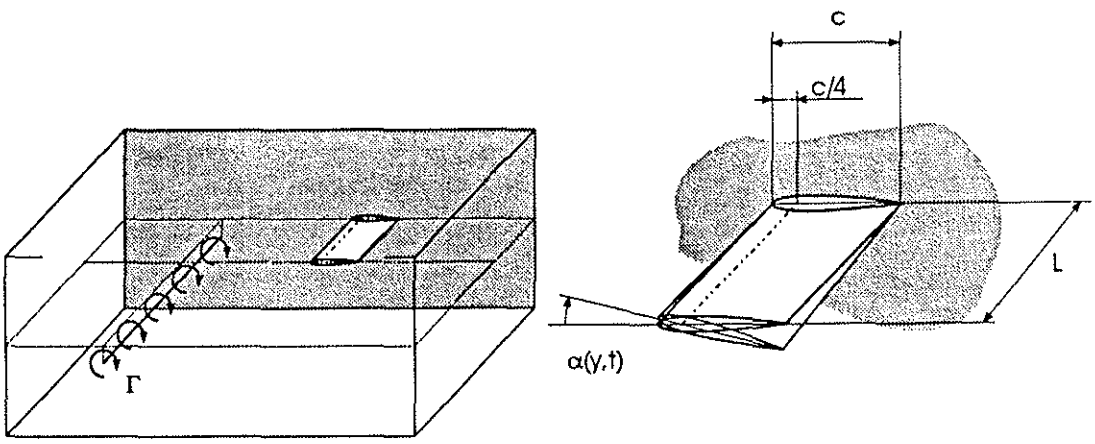

Figure 5: Interaction of a line vortex with a flexible blade (torsion, bending)

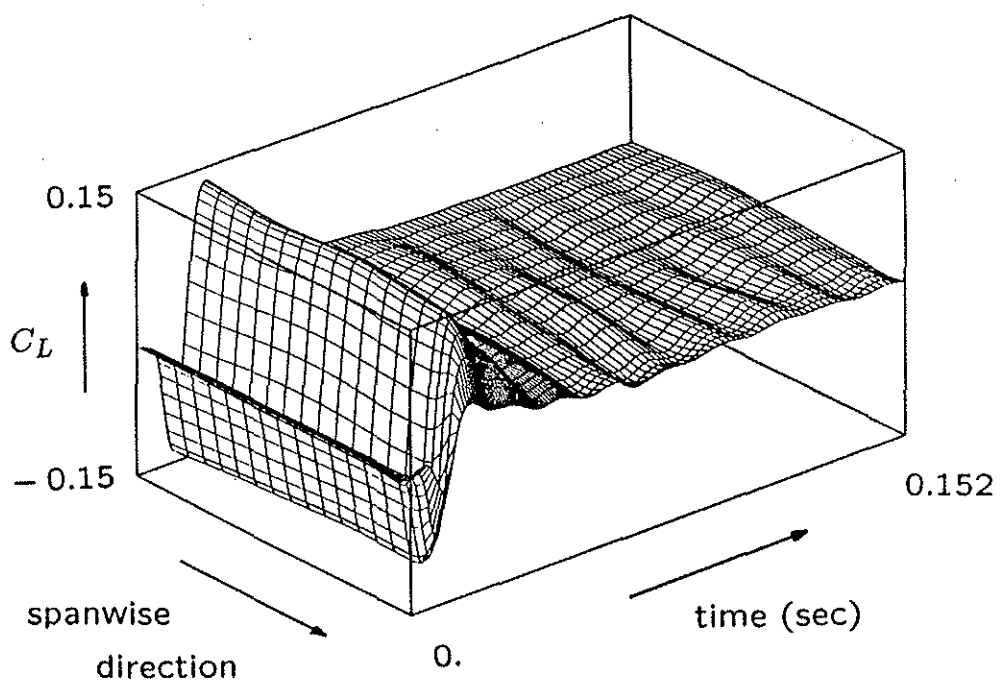

Figure 6: Computed lift coefficient for a flexible blade (M=0.73, Γ=0.4, y_w=0.26)

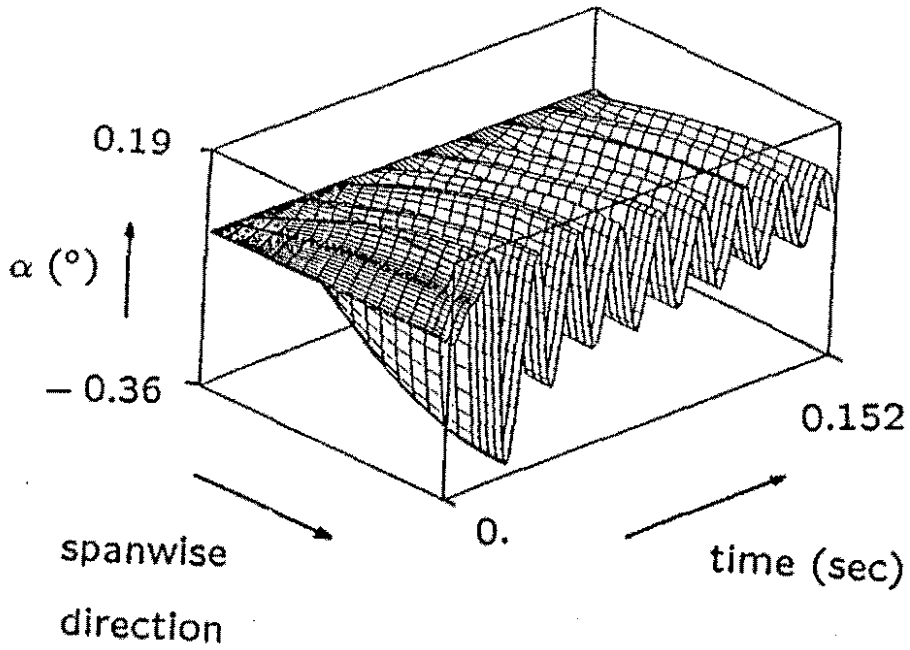

Figure 7: Angle of Attack versus time and spanwise direction

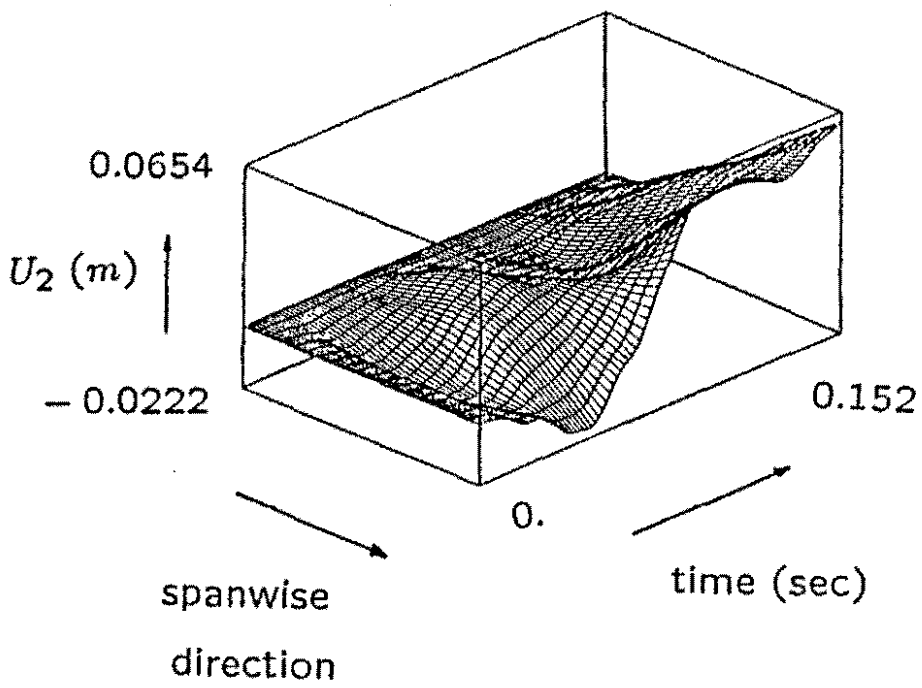

Figure 8: Deflection perpendicular to the undisturbed flow versus time and spanwise direction

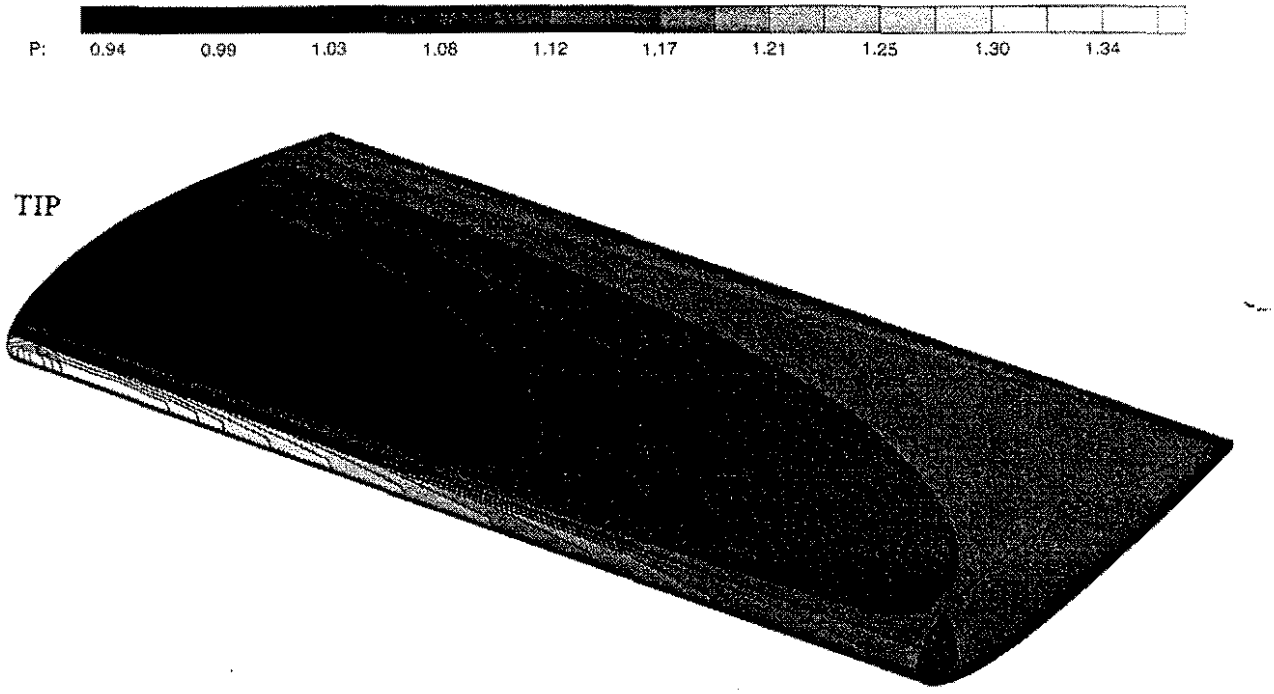

Figure 9: Steady pressure distribution about a rotating blade
(M_{TIP} = 0.7; NACA0012 cross-sections, aspect ratio A = 10)

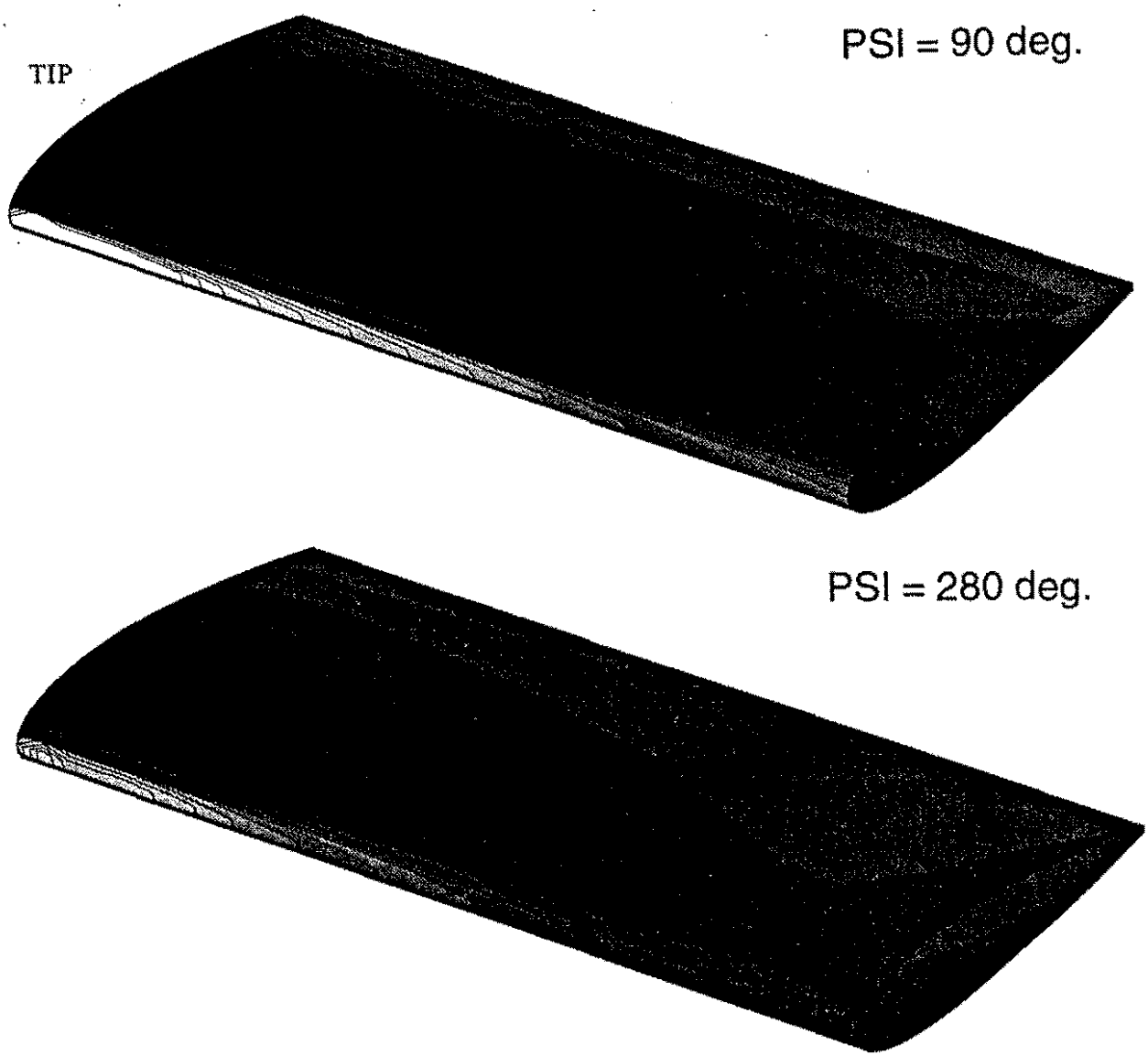

Figure 10: Unsteady pressure distribution about a rotating blade for two azimuthal angles PSI
(M_{TIP} = 0.7; NACA0012 cross-sections, aspect ratio A = 10, advance ratio μ=0.1)